Research Square

Preprints are preliminary reports that have not undergone peer review.
They should not be considered conclusive, used to inform clinical practice,
or referenced by the media as validated information.

Thermo-Mechanical Material Screening and Constraint-Based Optimization of an Automotive Clutch Using Response Surface Methodology

Trinh Phi Hoang

trinh.phihoang@eaut.edu.vn

East Asia University of Technology

Thanh Dinh Van

East Asia University of Technology

Article

Keywords: Automotive clutch, Thermo-mechanical analysis, Multiscale material homogenization, ANSYS Material Designer, Response surface methodology, Thermal constraint, Operating-condition optimization

Posted Date: November 16th, 2026

DOI: https://doi.org/10.21203/rs.3.rs-11421036/v1

License: This work is licensed under a Creative Commons Attribution 4.0 International License.
Read Full License

Additional Declarations: No competing interests reported.

Thermo-Mechanical Material Screening and Constraint-Based Optimization of an Automotive Clutch Using Response Surface Methodology

Phi Hoang Trinh
East Asia University of Technology
Trinh Van Bo Street, Bac Tu Liem District, Hanoi, Vietnam, 11900
trinh.phihoang@eaut.edu.vn
http://orcid.org/*0009-0004-6269-747X*
Dinh Van Thanh
East Asia University of Technology
Trinh Van Bo Street, Bac Tu Liem District, Hanoi, Vietnam, 11900
thanh.dinh@eaut.edu.vn
http://orcid.org/*0009-0009-5527-001X*

Corresponding author: Phi Hoang Trinh (trinh.phihoang@eaut.edu.vn

Author's order	*First Name*	*Middle name*	*Second Name*
1	*Trinh*	*Hoang*	*Phi*
2	*Thanh*	*Van*	*Dinh*

Abstract

This study presents an integrated computational framework combining multiscale material homogenization, transient thermo-mechanical analysis, and constraint-based optimization for automotive clutch design. Using ANSYS Material Designer, polymer matrix composites containing 15 vol.% Al_2O_3 were initially evaluated against a commercial friction material (COM_FM). Preliminary finite element analysis (FEA) indicated that increased thermal conductivity alone was insufficient to limit localized temperature rise. A composite containing 25 vol.% Al_2O_3 (PMC-M1-25) was therefore selected for further investigation. A 30-point design space was constructed using Latin hypercube sampling (LHS) with an optimal space-filling (OSF) configuration, considering clamping pressure (1.0–3.0 MPa), engine torque (150–350 N.m), and friction coefficient (0.25–0.40). Response surface methodology (RSM) was used to model global component deformation and peak interface temperature. The maximum sampled temperature reached 456.83 °C, highlighting the importance of evaluating thermally unfavorable operating conditions. Sensitivity analysis and response surface models were used to examine the effects of the operating parameters on the thermo-mechanical responses. Constraint-based optimization was then applied to identify operating conditions satisfying the prescribed thermal limit, followed by direct FEA verification of the selected condition. The proposed framework links composite material homogenization, thermo-mechanical response prediction, and constraint-based optimization to support the numerical assessment of automotive clutch operating conditions.

Keywords: Automotive clutch; Thermo-mechanical analysis; Multiscale material homogenization; ANSYS Material Designer; Response surface methodology; Thermal constraint; Operating-condition optimization.

1. INTRODUCTION

Automotive dry clutches transmit torque through frictional contact between the

clutch facings and mating surfaces. During engagement, frictional heat can produce localized temperature increases and thermal gradients, potentially affecting component deformation, frictional behavior, and service life [1–4]. Therefore, evaluating the coupled thermal and structural responses under different operating conditions is important for assessing clutch performance.

Polymer-based friction materials are widely used in clutch facings, but their relatively low thermal conductivity can limit heat dissipation. Aluminum oxide (Al_2O_3) is commonly considered a reinforcing filler because of its hardness and thermal stability [5-8]. However, the resulting material properties depend on filler content, particle distribution, and matrix–filler interactions. Numerical homogenization using representative volume elements (RVEs) provides a means of estimating effective material properties for subsequent component-level finite element analysis (FEA) [9-13].

Although thermo-mechanical FEA and response surface methodology (RSM) have been applied to engineering design and optimization, selecting operating conditions based on structural response alone may overlook unfavorable thermal conditions. Design of experiments (DOE), including Latin hypercube sampling (LHS) and optimal space-filling (OSF) strategies, can be used to explore the effects of multiple operating parameters and construct response models for optimization [14-25]. However, the thermal response must also be considered when identifying feasible operating conditions for a clutch incorporating polymer-based friction materials.

This study develops an integrated numerical framework combining material homogenization, transient thermo-mechanical FEA, and constraint-based optimization. Composites containing 15 vol.% Al_2O_3 are initially evaluated against a commercial friction material (COM_FM), followed by the selection of a composite containing 25 vol.% Al_2O_3 (PMC-M1-25) for further analysis. A 30-point LHS–OSF design is constructed using clamping pressure (1.0–3.0 MPa), engine torque (150–350 N.m), and friction coefficient (0.25–0.40) as input parameters. RSM is then used to model global component deformation and peak interface temperature, examine parameter effects, and identify operating conditions that satisfy the prescribed thermal constraint. The selected condition is subsequently evaluated using direct FEA.

The main contribution is the integration of homogenized composite properties with component-level thermo-mechanical analysis and thermal-constraint-based operating-condition selection. This approach provides a numerical basis for assessing the trade-off between structural deformation and temperature and for avoiding operating conditions that exceed the specified thermal limit.

1. MATHEMATICAL MODELING AND BOUNDARY CONDITIONS

2.1 Governing Equations for Transient Thermo-Mechanical Analysis

The transient thermal response of the clutch assembly is governed by the energy conservation equation:

$$\rho c \frac{\partial T}{\partial t} = \nabla.(k\nabla T) + q \quad (1)$$

where ρ is the material density, c_p is the specific heat capacity, T is the temperature, k is the thermal conductivity, and q is the volumetric heat-generation rate. When internal heat generation is neglected, the equation becomes

$$\rho c \frac{\partial T}{\partial t} = \nabla \cdot (k\nabla T) \quad (2)$$

The thermal field is subsequently used to evaluate the structural response under the applied mechanical loads. Assuming linear elastic behavior, the total strain is expressed as

$$\varepsilon = \varepsilon_e + \varepsilon_{th} \quad (3)$$

where the thermal strain is

$$\varepsilon_{th} = \alpha(T - T_{\text{rrr}}) \quad (4)$$

The stress–strain relationship is given by

$$\sigma = \mathrm{C}: \varepsilon_r \quad (5)$$

where ε, ε^{r} and ε^{tt} are the total, elastic, and thermal strain tensors, respectively; α is the coefficient of thermal expansion; T_{rrr} is the reference temperature; I is the identity tensor; σ is the stress tensor; and C is the elasticity tensor defined by Young's modulus and Poisson's ratio. For the Al_2O_3 reinforced polymer matrix composite, the effective thermal and mechanical properties obtained through numerical homogenization are assigned to the component-level finite element model. This links the material-scale characterization to the thermo-mechanical analysis of the clutch assembly.

2.2 Frictional Heating and Thermal Response at the Contact Interface

During clutch engagement, relative sliding between contacting surfaces generates frictional heat. The nominal frictional heat flux can be expressed as:

$$q_f'' = \mu \cdot p \cdot v_{\text{rrr}} \quad (6)$$

where ε,ε^{r} and ε^{tt} are the total, elastic, and thermal strain tensors, respectively; α is the coefficient of thermal expansion; T_{rrr} is the reference temperature; I is the identity tensor; σ is the stress tensor; and C is the elasticity tensor defined by Young's modulus and Poisson's ratio. For the Al_2O_3 reinforced polymer matrix composite, the effective thermal

and mechanical properties obtained through numerical homogenization are assigned to the component-level finite element model. This links the material-scale characterization to the thermo-mechanical analysis of the clutch assembly.

2.3 Frictional Heating and Thermal Response at the Contact Interface

During clutch engagement, relative sliding between contacting surfaces generates frictional heat. The nominal frictional heat flux can be expressed as:

$$q_f'' = \mu.p.v_{rrr} \tag{6}$$

where q_f'' is the frictional heat flux, μ is the friction coefficient, p is the local contact pressure, and v_{rrr} is the relative sliding velocity. For rotational contact:

$$v_{rrr} = r|\omega_1 - \omega_2| \tag{7}$$

where r is the radial distance from the rotation axis and ω_1 and ω_2 are the angular velocities of the contacting surfaces. The generated heat is distributed between the contacting components according to their thermal properties and interface conditions. The heat flux entering the composite friction material can be represented as:

$$q_c'' = \beta_c \cdot q_f'' \tag{8}$$

where β_c is the heat partition coefficient. Under idealized contact conditions, the partition coefficient can be estimated from the thermal effusivities of the composite and steel. However, the actual heat distribution depends on the contact conditions and thermal properties used in the model. The thermal response is characterized by the peak temperature at the friction interface. This response is denoted by Y_2 and is evaluated over the prescribed operating-parameter space. The resulting temperature values provide the basis for identifying operating conditions that satisfy the specified thermal constraint during response surface modeling and optimization.

2.4 Structural Boundary Conditions and Contact Mechanics

The mechanical boundary conditions represent the mounting constraints and clamping action of the clutch assembly. The flywheel mounting surface is fixed by imposing:

$$u = 0 \tag{9}$$

where u is the displacement vector. For a uniformly distributed nominal clamping pressure p_c over an annular contact area, the corresponding axial force is:

$$F_c = p_c A_c = \pi p_c (R_o^2 - R_i^2) \tag{10}$$

where F_c is the axial clamping force, A_c is the effective contact area, and R_o and R_i

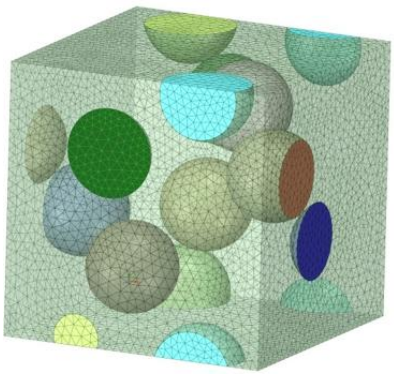
are the outer and inner radii of the contact region, respectively. Frictional contact between the mating components is modeled using the Augmented Lagrange formulation where specified in the finite element setup. The contact solution accounts for the local pressure distribution and mechanical interaction between the contacting surfaces. The global component deformation Y_1, and peak interface temperature, Y_2, are selected as the principal responses for subsequent response surface modeling. These responses are evaluated for combinations of clamping pressure, engine torque, and friction coefficient within the prescribed design ranges. The resulting models are then used to assess the structural and thermal responses and identify operating conditions that satisfy the specified constraints.

3. NUMERICAL MATERIAL DESIGN AND MICROSTRUCTURAL HOMOGENIZATION

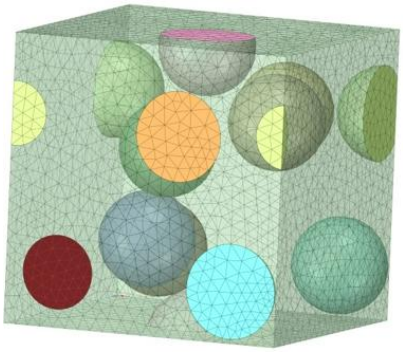
3.1. Initial Material Design and Numerical Homogenizatio

Numerical homogenization was performed using ANSYS Material Designer to estimate the effective thermo-mechanical properties of two Al_2O_3 reinforced polymer matrix composites and compare them with a commercial organic friction material (COM-FM). The candidate composites, designated PMC-M1 and PMC-M2, contained 15 vol.% spherical Al_2O_3 microparticles with a nominal diameter of 10 μm embedded in

Hybrid_Matrix M1 and Hybrid_Matrix M2, respectively. Representative volume elements (RVEs) containing randomly distributed particles were constructed to represent the composite microstructures. Figure 1 shows the RVE configurations and corresponding finite element meshes. Periodic boundary conditions (PBCs) were applied to opposing faces where supported by the homogenization setup to estimate the effective thermo-mechanical properties [26].



a,



b,

Figure 1. RVE configurations and finite element meshes of the composites containing 15 vol.% Al_2O_3 microparticles: (a) PMC-M1 and (b) PMC-M2.

The effective properties of the candidate composites and the commercial baseline are summarized in Table 1.

Table 1. Effective thermo-mechanical properties of the candidate friction materials.

Material property	Symbol	Unit	COM-FM (Baseline)	PMC-M1	PMC-M2
Density	ρ	kg/m³	2000	1852.6	1812.5
Young's modulus	E	GPa	4.2	11.49	7.77
Poisson's ratio	ν	–	0.27	0.31	0.32
Thermal conductivity	k	W/(m·K)	0.55	1.05	2.15
Coefficient of thermal expansion	α	K^{-1}	$1{,}80x10^{-5}$	$2{,}51x10^{-5}$	$2{,}01x10^{-5}$
Specific heat capacity	c_p	J/(kg·K)	950	1146.5	1105

Both reinforced composites exhibit higher Young's modulus and thermal conductivity than COM-FM. PMC-M1 has the highest Young's modulus, at 11.49 GPa, representing an increase of approximately 173.6% relative to the baseline. Its thermal conductivity is 1.05 W/(m·K), approximately 90.9% higher than that of COM-FM.

PMC-M2 exhibits the highest thermal conductivity among the initial candidates, reaching 2.15 W/(m·K). This value is approximately 290.9% higher than that of COM-FM and 104.8% higher than that of PMC-M1. However, its Young's modulus is lower than that of PMC-M1. The two composites therefore exhibit different combinations of effective stiffness and thermal conductivity. These results indicate that the effective properties alone are insufficient to establish the suitability of a friction material for clutch applications. Component-level thermo-mechanical simulations are required to evaluate how the material properties influence temperature and deformation under the prescribed operating

conditions.

3.2 Physics-Based Material Screening and Selection of PMC-M1-25

A preliminary transient thermo-mechanical analysis was conducted under the prescribed baseline operating conditions to compare the candidate materials and select a formulation for the subsequent parametric investigation. The predicted responses and solver status are summarized in Table 2.

Table 2. Preliminary transient screening results for the candidate friction materials.

Design point	Material	Maximum total deformation, P_1 (mm)	Maximum component deformation, P_4 (mm)	Peak interface temperatur, P_7 (°C)	Peak mating temperatur, P_{10} (°C)	Solver status
DP1	COM-FM (baseline)	0.387	0.387	407.75	407.75	Converged
DP2	PMC-M1 (15% AL_2O_3)	0.455	0.401	246.32	246.32	Converged
DP3	PMC-M2 (15% AL_2O_3)	N/A	N/A	152.87	152.87	Non converged structural solution
DP0	PMC-M1-25 (25% AL_2O_3)	0.470	0.403	204.31	204.31	Converged

The commercial baseline produced a peak interface temperature of 407.75 °C. Replacing COM-FM with PMC-M1 reduced the predicted peak temperature to 246.32 °C, a reduction of approximately 39.6%. However, the maximum total deformation increased from 0.387 to 0.455 mm, indicating that the improved thermal response was accompanied by a modest increase in predicted deformation.

PMC-M2 produced a lower peak interface temperature of 152.87 °C. However, its structural solution did not converge, and no valid deformation results were obtained. Consequently, the available results are insufficient to establish its overall thermo-mechanical suitability. Non-convergence indicates that a reliable structural solution was not obtained under the current numerical setup; it does not, by itself, demonstrate physical failure or identify the cause of the numerical problem. To investigate the effect of a higher ceramic-particle content, the Hybrid_Matrix M1 formulation was retained and the Al_2O_3 volume fraction was increased from 15 to 25 vol.%, producing PMC-M1-25. Under the prescribed baseline conditions, this formulation yielded a converged solution, with a maximum total deformation of 0.470mm, a maximum component deformation of 0.403mm, and a peak interface temperature of 204.31°C.

Relative to PMC-M1, PMC-M1-25 reduced the predicted peak interface

temperature by approximately 17.1%, while the maximum total deformation increased by 0.015 mm. Compared with COM-FM, the peak temperature decreased by approximately 49.9%. Based on this preliminary comparison, PMC-M1-25 was selected for the subsequent parametric study because it provided a lower predicted interface temperature than COM-FM and PMC-M1 while yielding a converged structural solution. This selection reflects the numerical results under the specified baseline conditions and does not establish experimental thermal stability or global material optimality. The influence of operating parameters on the thermal and structural responses is investigated in the following sections.

3.3 Microstructural Representation and Effective Properties of PMC-M1-25

Following the preliminary screening, the effective thermo-mechanical properties of PMC-M1-25 were estimated using an RVE model in ANSYS Material Designer. The model contained randomly distributed spherical Al_2O_3 particles with a nominal diameter of 10 μm and a volume fraction of 25%, embedded in the Hybrid_Matrix M1 formulation.

Figure 2 shows the three-dimensional RVE and its finite element mesh. The microstructure was discretized using tetrahedral elements to represent the particle and matrix phases. Periodic boundary conditions were applied to opposing faces where supported by the selected homogenization procedure.

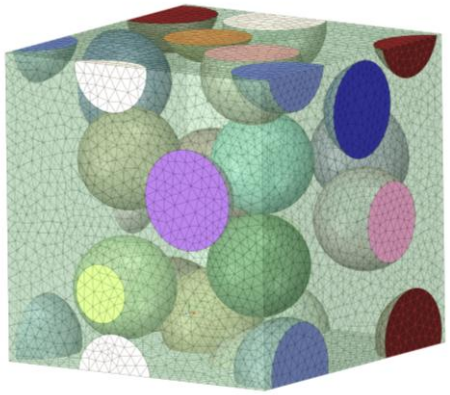


Figure 2. Representative volume element and finite element mesh of PMC-M1-25.

The effective properties obtained from the RVE analysis are summarized in Table 3. The predicted Young's moduli were 14,556, 14,432, and 14,476 MPa along the three principal directions. The corresponding Poisson's ratios were 0.2899, 0.2971, and 0.30344. The effective density was 2.0934×10^{-9} t/mm³, equivalent to 2093.4 kg/m³.

The effective thermal conductivities were 1.361, 1.3602, and 1.3808 W/(m·K) along the three principal directions. The coefficients of thermal expansion were 2.2555×10^{-5} 2.2540×10^{-5} and 2.2160×10^{-5} K^{-1} along the X, Y, and Z directions, respectively. The effective specific heat capacity was 1088.8 J/(kg·K).

Table 3. Effective physical, mechanical, and thermal properties of PMC-M1-25 obtained from RVE homogenization.

Property	Symbol	Value	Unit
Al_2O_3 particle volume fraction	V_f	25	vol.%
Al_2O_3 particle diameter	d_p	10	μm
Density	ρ	2093.4	kg/m³
Young's modulus, direction 1	E_1	14,556	MPa
Young's modulus, direction 2	E_2	14,432	MPa
Young's modulus, direction 3	E_3	14,476	MPa
Poisson's ratio, direction 1–2	ν_{12}	0.2899	–
Poisson's ratio, direction 1–3	ν_{13}	0.2971	–
Poisson's ratio, direction 2–3	ν_{23}	0.30344	–
Thermal conductivity, direction 1	k_1	1.361	W/(m·K)
Thermal conductivity, direction 2	k_2	1.3602	W/(m·K)
Thermal conductivity, direction 3	k_3	1.3808	W/(m·K)
Coefficient of thermal expansion, X direction	α_X	2.2555×10^{-5}	K^{-1}
Coefficient of thermal expansion, Y direction	α_Y	2.2540×10^{-5}	K^{-1}
Coefficient of thermal expansion, Z direction	α_Z	2.2160×10^{-5}	K^{-1}
Specific heat capacity	c_p	1088.8	J/(kg·K)

The directional Young's moduli differ by less than 1% relative to their mean value, while the maximum difference among the three thermal conductivity values is approximately 1.5% relative to their mean. These results indicate an approximately quasi-isotropic effective response in stiffness and thermal conductivity for the modeled RVE. However, similarity among these properties alone does not establish complete isotropy of the full constitutive behavior.

The homogenized properties of PMC-M1-25 were assigned to the component-level clutch model for the subsequent parametric analysis. The predicted global component deformation and peak interface temperature were then evaluated over the prescribed operating-parameter space to construct the response surface models and assess the thermal

and structural constraints.

4. FINITE ELEMENT MODELLING AND SIMULATION SETUP

4.1 Geometric Model and Computational Domain

A three-dimensional finite element model of an automotive dry clutch assembly was developed in ANSYS Workbench to investigate its thermal and structural responses under prescribed operating conditions. The model represented the main components involved in torque transmission and frictional contact, including the flywheel, composite friction lining, and pressure plate. The friction lining was assigned the effective material properties of PMC-M1-25, containing 25 vol.% Al_2O_3 particles, as determined through numerical homogenization in ANSYS Material Designer (Section 3).

The composite friction lining was modelled as an annular component positioned between the flywheel and pressure plate. Its inner and outer radii were denoted by R_i and R_0 respectively. The component geometry, material assignments, and contact interfaces were defined consistently for the baseline and parametric simulations. The numerical model was used to evaluate two principal responses: the maximum total deformation of the assembly, Y_1 and the maximum temperature, Y_2. These responses were subsequently used to assess the influence of the operating parameters and construct the response surface models.

4.2 Finite Element Mesh

The assembled geometry was discretized using a nominal global element size of 3 mm. Tetrahedral and hexahedral elements were employed according to the geometric characteristics and meshing requirements of the individual components. Sweep meshing was applied to suitable disc-shaped regions, while local mesh controls were introduced around the friction-contact regions to represent the relevant geometric features.

The resulting finite element mesh contained 312,232 elements and 601,371 nodes. This discretization was used for the baseline simulation and the subsequent parametric analyses. The same general meshing strategy was maintained across the investigated design points to ensure consistency in the numerical comparisons.

The reported element size and mesh statistics describe the discretization used in this study. Since a separate mesh-convergence assessment has not been established in the reported results, the mesh is not claimed to be mesh-independent.

4.3 Applied Loads, Boundary Conditions, and Contact Definitions

The mechanical loading and boundary conditions were defined to represent the prescribed operating conditions of the dry clutch assembly. For the baseline design point, DP0, a clamping pressure of 1.5 MPa was applied to the actuation face of the pressure plate, while a torque of 320 N·m was applied to the designated torque-transmission region. The friction coefficient at the contact interfaces was set to 0.325. These values defined the reference conditions for evaluating the thermal and structural responses of the PMC-M1-25 composite lining. Support conditions were assigned to the appropriate central and mounting regions to constrain rigid-body motion and represent the intended mechanical constraints. Cylindrical supports were used where applicable, with the constrained degrees of freedom defined according to the corresponding support locations and the intended behaviour of the assembly. The applied loads and structural boundary conditions are illustrated in Fig. 3.

Frictional contact interactions were defined between the composite friction lining and the opposing surfaces of the flywheel and pressure plate. The Augmented Lagrange formulation was used for contact modelling. The reference friction coefficient of 0.325 was applied at DP0, while the friction coefficient was varied within the prescribed range during the parametric study. The general contact formulation and modelling strategy were maintained across the investigated design points.

The thermal response was evaluated using the thermal loading and boundary conditions specified in the ANSYS model. The resulting temperature field was used in the structural assessment to account for thermally induced deformation. The thermal-loading procedure and the transfer of the temperature field were maintained consistently across the investigated design points.

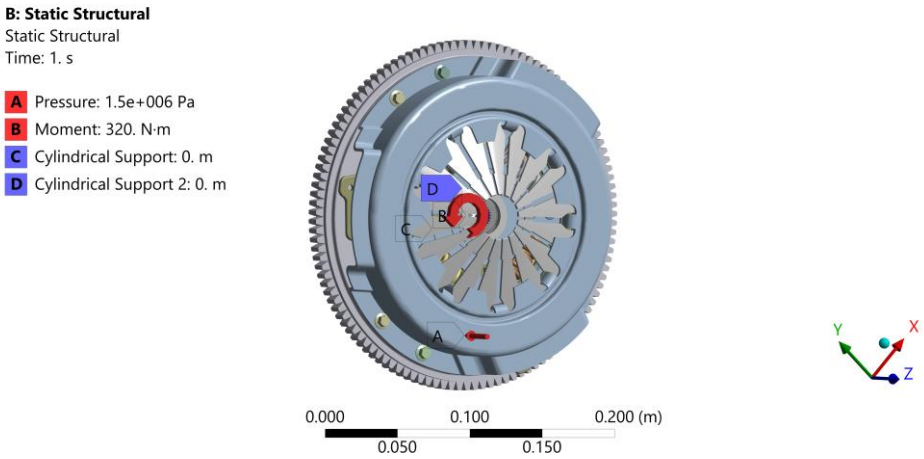
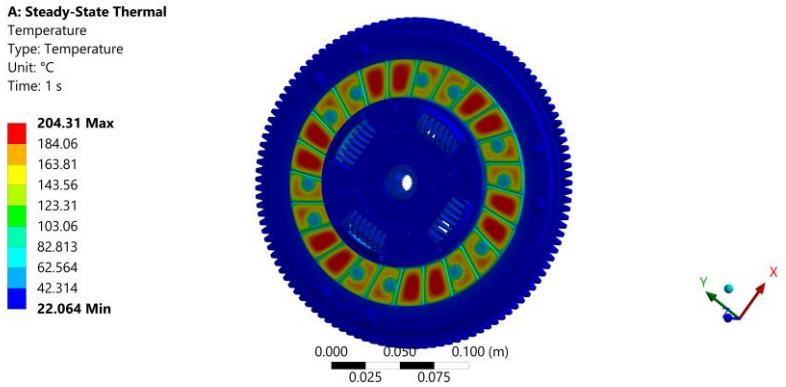


Figure 3. Applied mechanical loads and structural boundary conditions of the automotive dry clutch assembly in ANSYS Mechanical.

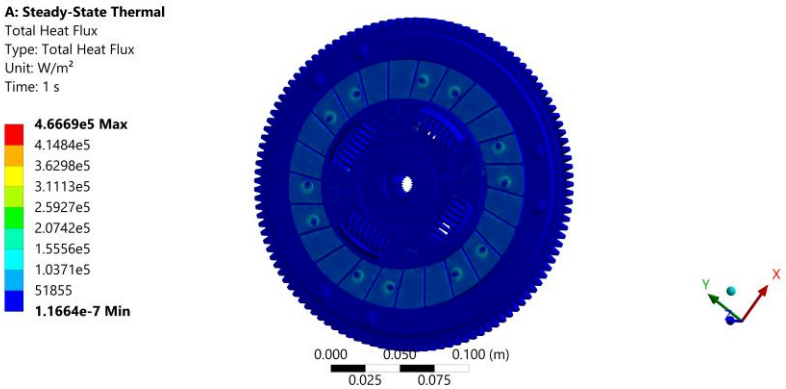
4.4 Baseline Simulation Results and Post-Processing

A baseline simulation was performed to establish the reference thermal and structural responses of the selected PMC-M1-25 composite clutch assembly. The baseline operating parameters were a clamping pressure of 1.5 MPa, a transmitted torque of 320 N·m, and a friction coefficient of 0.325. This operating condition was designated as DP0. The simulation predicted a maximum temperature of 204.31°C and a minimum temperature of 22.064°C. The maximum total deformation was 0.47016 mm, while the maximum total heat flux was 4.6669×10^5 W/m². These values were used as reference results for comparison with the subsequent parametric simulations.

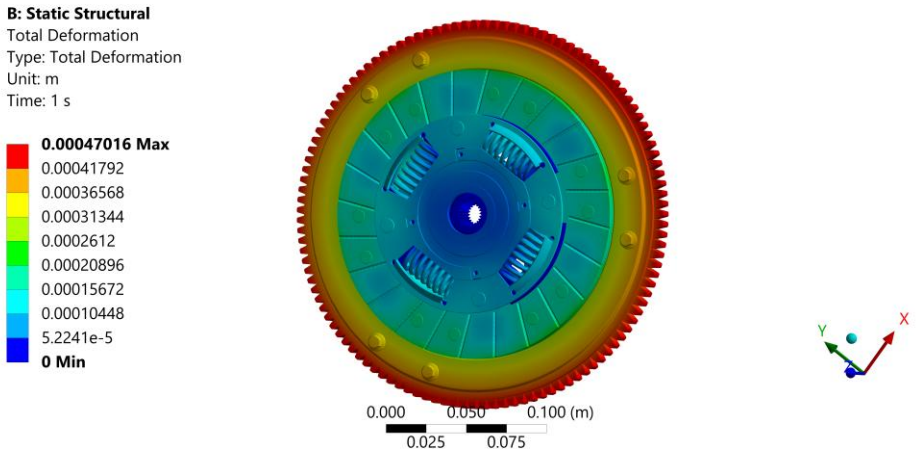
Figure 4 presents the temperature, total heat-flux, and total-deformation distributions obtained for DP0. To improve the visibility of the numerical results, selected components and structural details, including the clutch housing, diaphragm spring, and pressure plate, were hidden in the post-processing views where necessary. This presentation approach allows the relevant result fields to be observed more clearly. Hiding a component in a post-processing view does not necessarily mean that it was excluded from the computational model; the actual model scope is determined by the components included in the ANSYS analysis.



a,



b,



c,

Note: *Auxiliary components, including the clutch housing and diaphragm spring, are hidden in the post-processing views to improve the visualization of the friction lining.*

Figure 4. Predicted thermo-mechanical field distributions of the PMC-M1-25 composite friction lining under the baseline reference condition (DP0): (a) temperature distribution; (b) total heat-flux distribution; and (c) total-deformation distribution.

The baseline simulation provides the reference condition for the subsequent 30-point Latin hypercube sampling (LHS) design. In this parametric study, the clamping pressure, transmitted torque, and friction coefficient were varied within the ranges of 1–3 MPa, 150-350 N·m, and 0.25–0.40, respectively. The resulting finite element dataset was used to construct response surface models and evaluate the sensitivity of the maximum total deformation Y_1 and maximum temperature Y_2, to variations in the operating parameters. The response surface models were subsequently used to identify operating conditions that satisfy the prescribed thermal constraint while accounting for the structural response of the clutch friction lining.

5. RESULTS AND DISCUSSION

5.1 Parametric Evaluation of the LHS-OSF Design Space and Thermal Response Screening

A 30-point Latin hypercube sampling design combined with an optimal space-filling (LHS-OSF) strategy was used to investigate the thermo-mechanical response of the automotive dry clutch assembly incorporating the PMC-M1-25 composite friction lining. Three input parameters were considered: clamping pressure P_{19}, applied torque P_{20}, and friction coefficient P_{21}. The investigated ranges were 1–3 MPa, 150–350 N·m, and 0.25–0.40, respectively. The primary responses were maximum assembly deformation $Y_1=P_1$

and maximum temperature Y_2=P_7. The complete sampling matrix and the corresponding simulation results are presented in Table 4. The table provides the numerical basis for the subsequent response-surface construction, sensitivity assessment, and multi-objective optimization.

Table 4. Complete 30-point LHS-OSF design matrix and corresponding thermo-mechanical responses of the dry clutch assembly using PMC-M1-25

Design point	Clamping pressure, P_{19} (MPa)	Applied torque, P_{20} (N·m)	Friction coefficient, P_{21}	Maximum assembly deformation, Y_1 (mm)	Maximum temperature, Y_2 (°C)
DP1	2.567	306.67	0.3475	0.653	383.36
DP2	1.167	153.33	0.2625	0.396	146.08
DP3	1.197	273.33	0.2925	0.537	255.06
DP4	2.033	346.67	0.3725	0.574	328.87
DP5	2.767	186.67	0.3525	0.679	417.13
DP6	2.633	213.33	0.3275	0.650	371.41
DP7	2.833	286.67	0.3075	0.682	374.99
DP8	2.100	206.67	0.2725	0.548	253.85
DP9	2.700	300.00	0.3975	0.691	456.83
DP10	1.100	320.00	0.3825	0.416	192.47
DP11	1.033	280.00	0.3125	0.394	152.83
DP12	2.500	253.33	0.2675	0.613	292.95
DP13	1.833	260.00	0.3225	0.521	261.55
DP14	1.300	266.67	0.3425	0.437	202.39
DP15	1.767	200.00	0.3875	0.517	299.36
DP16	2.433	220.00	0.2975	0.609	315.30
DP17	2.967	180.00	0.2825	0.687	361.55
DP18	1.367	160.00	0.3175	0.436	197.80
DP19	2.167	173.33	0.3675	0.580	344.60
DP20	1.567	233.33	0.3375	0.477	236.22

DP21	1.233	340.00	0.2525	0.427	148.17
DP22	1.433	293.33	0.3025	0.457	197.67
DP23	2.300	313.33	0.2575	0.586	261.95
DP24	1.700	240.00	0.3625	0.504	271.68
DP25	2.900	246.67	0.3325	0.698	412.67
DP26	2.233	193.33	0.3775	0.596	363.58
DP27	1.633	326.67	0.3925	0.508	281.74
DP28	1.900	226.67	0.2875	0.521	243.31
DP29	2.367	333.33	0.2775	0.603	288.08
DP30	1.500	166.67	0.3575	0.463	239.26

Across the 30 sampled design points, the maximum temperature ranged from 146.08°C to 456.83°C, while the maximum assembly deformation ranged from 0.394 to 0.698 mm. These ranges demonstrate that the predicted thermo-mechanical response varied substantially across the investigated parameter space.

DP2 produced the lowest temperature among the sampled points, at 146.08°C, together with a maximum assembly deformation of 0.396 mm. This response corresponded to a clamping pressure of 1.167 MPa, an applied torque of 153.33 N.m, and a friction coefficient of 0.2625. In contrast, DP9 produced the highest sampled temperature, 456.83°C, with a deformation of 0.691 mm. Its input conditions were 2.700 MPa, 300 N.m, and a friction coefficient of 0.3975. DP25 yielded the largest sampled deformation, 0.698 mm, at a clamping pressure of 2.900 MPa, an applied torque of 246.67 N.m, and a friction coefficient of 0.3325. The comparison between these design points indicates that the input parameters jointly influence the predicted response. However, the individual contribution of each parameter cannot be determined from these three cases alone because the input combinations differ simultaneously. The response-surface and sensitivity analyses presented in the following sections are therefore used to examine the parameter effects over the investigated design space.

A temperature threshold of 250°C was adopted for the constrained optimization based on previously published studies of the thermal behavior of dry friction clutches and friction lining materials [27,28]. In particular, Jabbar et al. [27] discussed 250°C as a relevant service-temperature limit for certain woven friction materials, while Pisaturo and Senatore [28] investigated the temperature field developed during dry-clutch engagement. Accordingly, the 250°C threshold was used in the present study as a literature-informed

design constraint for screening the simulated operating conditions. This value is not assumed to represent a verified continuous operating-temperature limit for PMC-M1-25, because its specific thermal limits have not been experimentally established.

5.2. Metamodel Verification and Statistical Reliability

Response-surface metamodels were developed to approximate the relationships between the input parameters and the thermo-mechanical responses. Their statistical performance was assessed using the coefficient of determination R_2, adjusted coefficient of determination R^2_{adj} predicted coefficient of determination R^2_{pred} and root-mean-square error (RMSE).

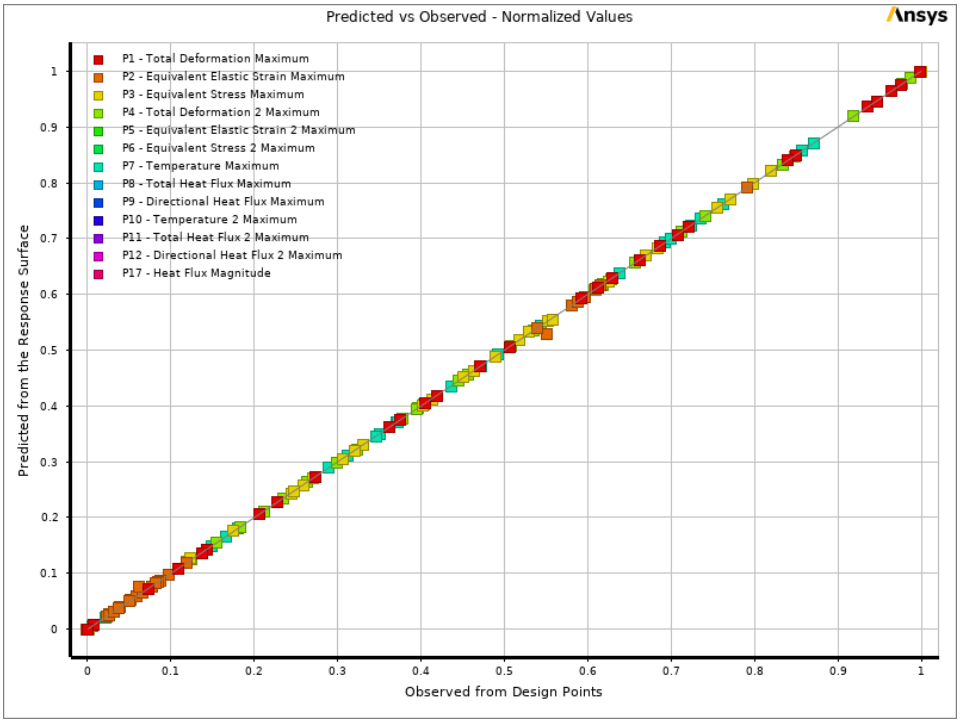


Figure 5. Predicted-versus-observed response plots for the developed response-surface metamodels.

The predicted-versus-observed plots in Fig.5 provide a visual assessment of the agreement between the metamodel predictions and the simulation results. The corresponding statistical indicators are summarized in Table 5.

Table 5. Statistical performance of the response-surface metamodels

Response	R^2	Adjusted R^2	Predicted R^2	RMSE
Maximum total deformation, P_1	0.9958	0.9942	0.9915	4.28×10^{-6}
Maximum component deformation, P_4	0.9946	0.9931	0.9898	3.71×10^{-6}
Peak contact temperature, P_7	0.9986	0.9979	0.9962	1.24×10^{-1}

Peak mating temperature, P_{10}	0.9984	0.9975	0.9959	$1.31x10^{-1}$
Maximum total heat flux, P_8	0.9962	0.9948	0.9923	$2.85x10^{-1}$
Maximum directional heat flux, P_{12}	0.9951	0.9935	0.9904	$3.02x10^{-1}$
Heat-flux magnitude, P_{17}	0.9973	0.9961	0.9938	$2.14x10^{-1}$

All responses had R^2 values above 0.994, while the adjusted and predicted R^2 values were also high. These results indicate that the fitted metamodels represented the sampled simulation data closely and showed good predictive statistics within the investigated design space. Nevertheless, a high R^2 value alone is not sufficient to establish the accuracy of an optimized solution. The predictive performance should also be evaluated by comparing metamodel predictions with direct finite-element analysis (FEA) results at the selected operating conditions. In addition, the units associated with the reported RMSE values for deformation and heat flux should be confirmed from the original DesignXplorer output before the RMSE magnitudes are interpreted quantitatively.

The metamodels were consequently used as computationally efficient approximations for exploring parameter interactions and identifying candidate solutions. Their predictions should be interpreted within the ranges of pressure, torque, and friction coefficient used to construct the sampling design; extrapolation beyond these ranges is not established by the present analysis.

5.3. Global Sensitivity Analysis

Global sensitivity analysis was performed to assess the relative influence of clamping pressure, applied torque, and friction coefficient on the predicted thermo-mechanical responses. This analysis complements the individual design-point comparisons by evaluating parameter influence across the investigated design space. For the thermal response, the reported sensitivity results attributed approximately 68% of the variation to clamping pressure and 32% to the friction coefficient, while the contribution associated with applied torque was close to zero. Within the present model and parameter ranges, these results identify clamping pressure as the leading parameter associated with the predicted thermal response, followed by friction coefficient.

For the structural response, clamping pressure was also reported as the dominant parameter, accounting for approximately 77–86% of the sensitivity associated with the deformation responses. The reported torque contribution was below 5%. These percentages should be interpreted as model-based sensitivity indicators rather than universal physical contributions. Their meaning depends on the sensitivity definition used by the software and on the parameter ranges included in the analysis. The low reported sensitivity to torque warrants particular care in interpretation. It does not establish that torque has no physical effect on clutch behaviour. Instead, it indicates that the current model's sensitivity analysis

assigned a relatively small contribution to torque over the selected design space. The result should therefore be considered alongside the response surfaces and direct FEA results.

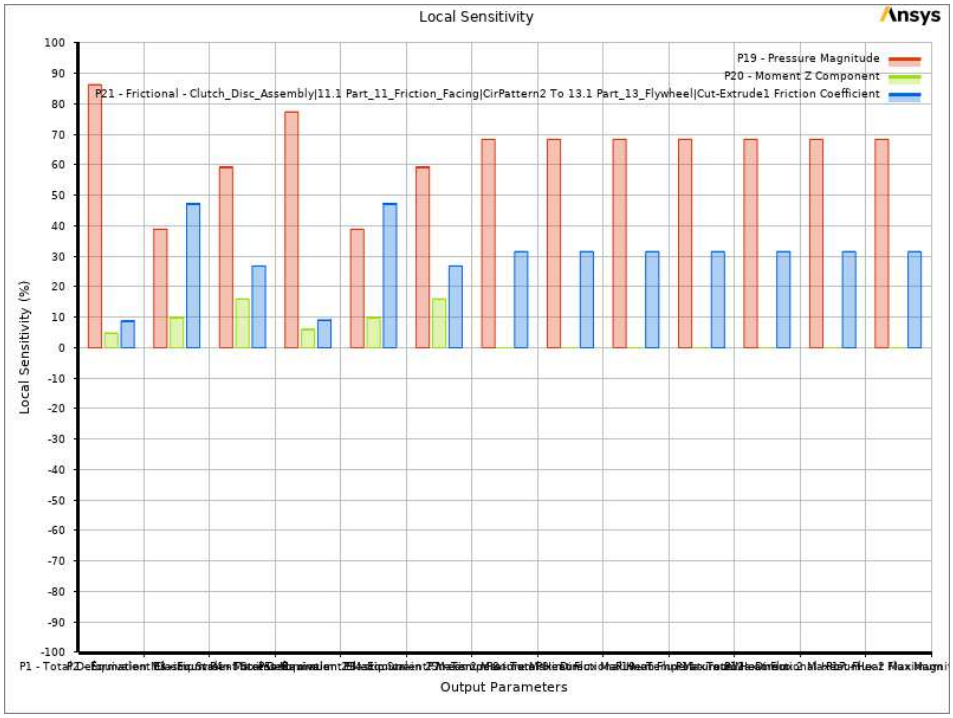


Figure 6. Global sensitivity of the thermo-mechanical responses to clamping pressure, applied torque, and friction coefficient.

Fig. 6 presents the reported relative sensitivities of the selected responses. These results help identify which input parameters deserve closer attention during design exploration. However, the sensitivity percentages should not be interpreted as independent causal effects unless the underlying sensitivity metric explicitly supports that interpretation.

5.4. Response Point Evaluation Using a Spider Chart

A spider chart was used to compare the selected response indicators across the evaluated design points. The chart provides a compact visual representation of the relative response levels and complements the numerical results in Table 3.

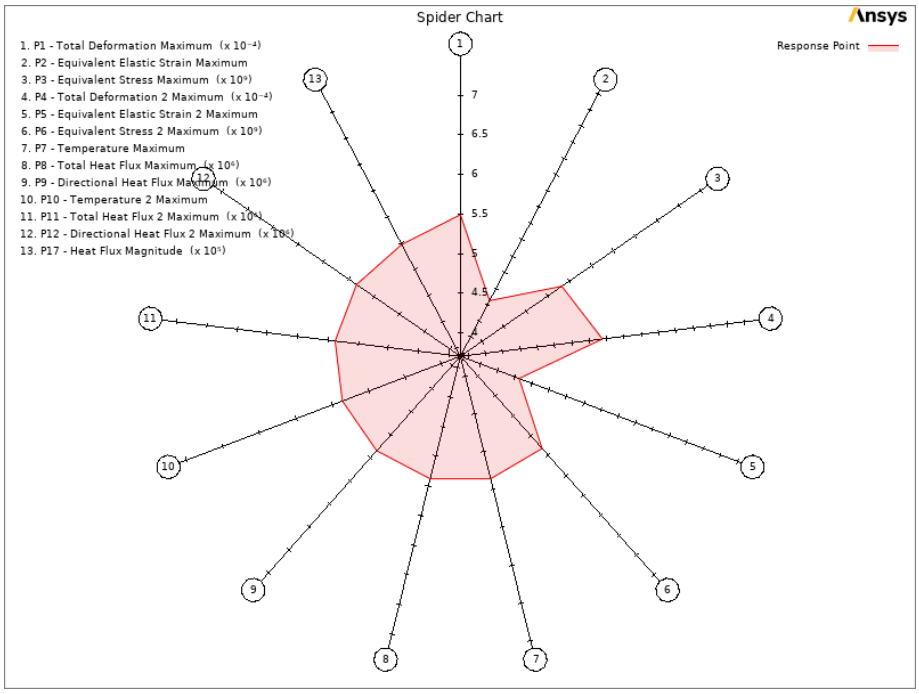
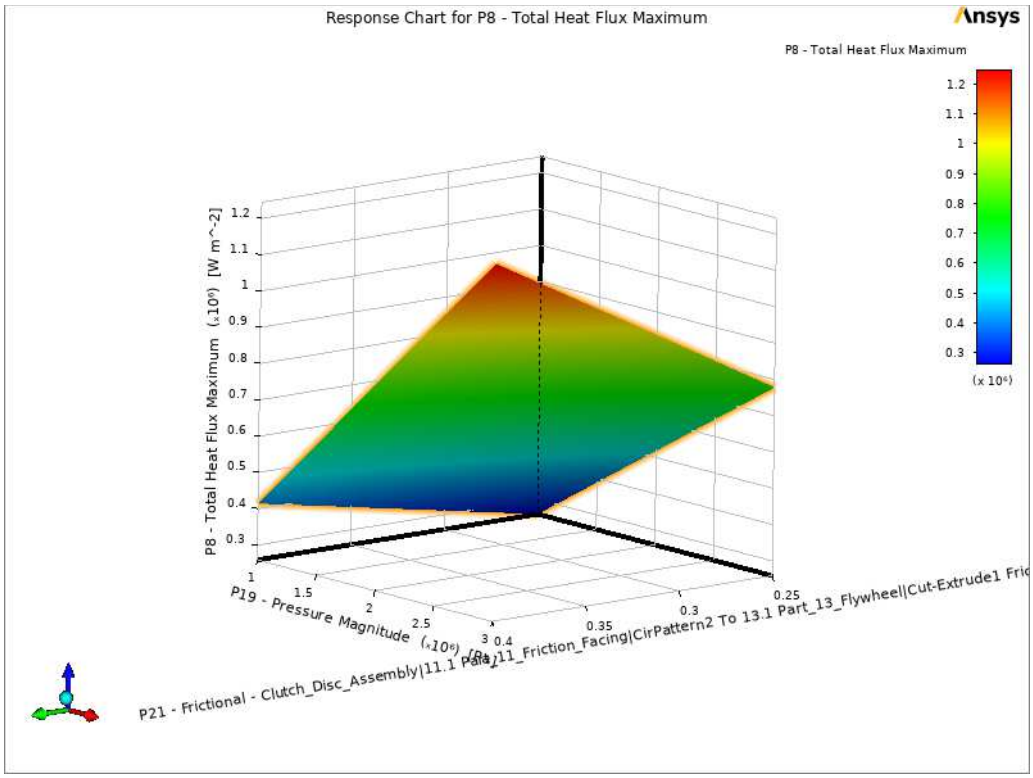


Figure 7. Spider-chart comparison of normalized thermo-mechanical response indicators at the selected design points.

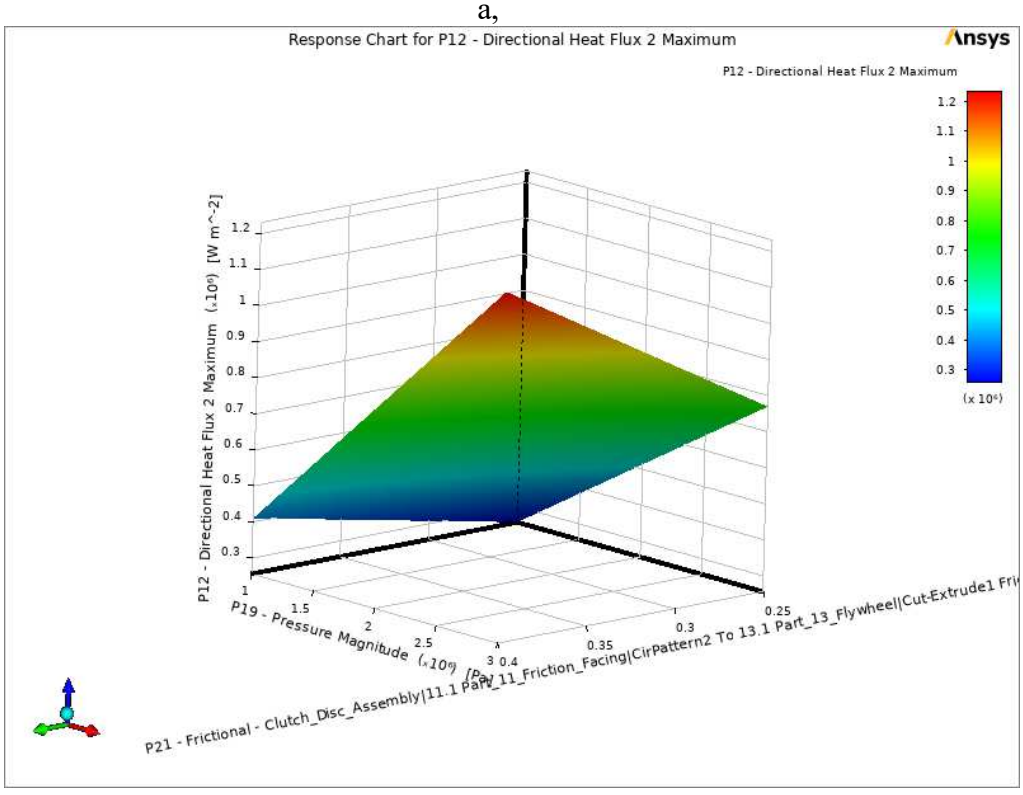
Because the response variables have different physical units and numerical ranges, normalization is necessary for plotting them on a common radial scale. The resulting chart is therefore intended for relative comparison rather than direct quantitative comparison between different response types. The spider chart should be interpreted together with the original numerical values. In particular, a larger normalized radius indicates a larger normalized value under the adopted normalization procedure; it does not, on its own, establish a thermal hotspot, a failure location, or a material safety margin. The numerical response ranges in Table 3 remain the primary basis for interpreting the sampled design points.

5.5. Response Surface Metamodeling and Three-Dimensional Interaction Analysis

Three-dimensional response surfaces were used to visualize the combined influence of the design parameters on the predicted heat-flux, temperature, and deformation responses. These surfaces provide a more continuous view of the metamodelled design space than the discrete sampling points alone.



a,

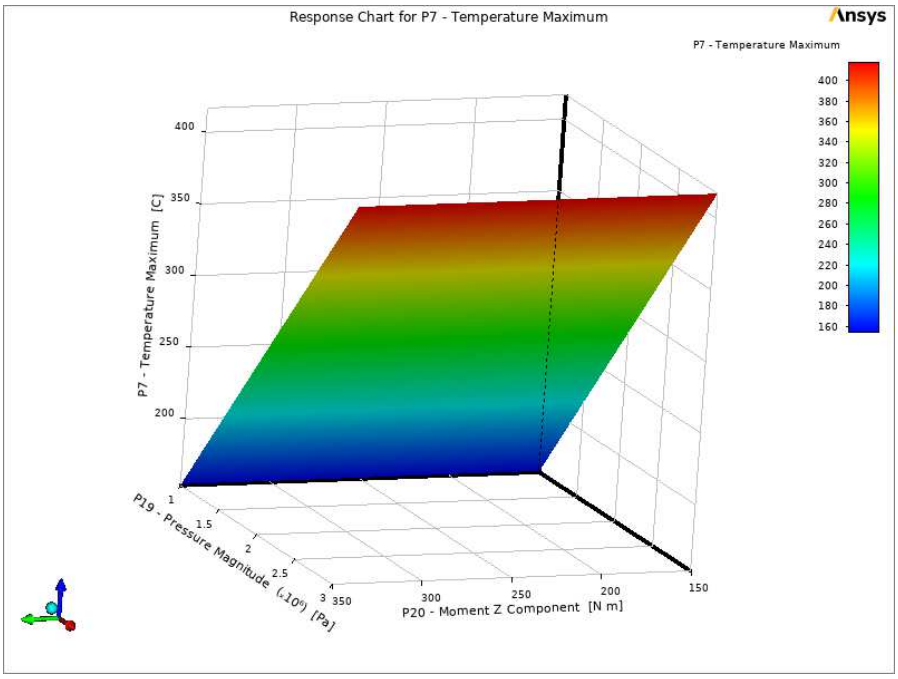


b,

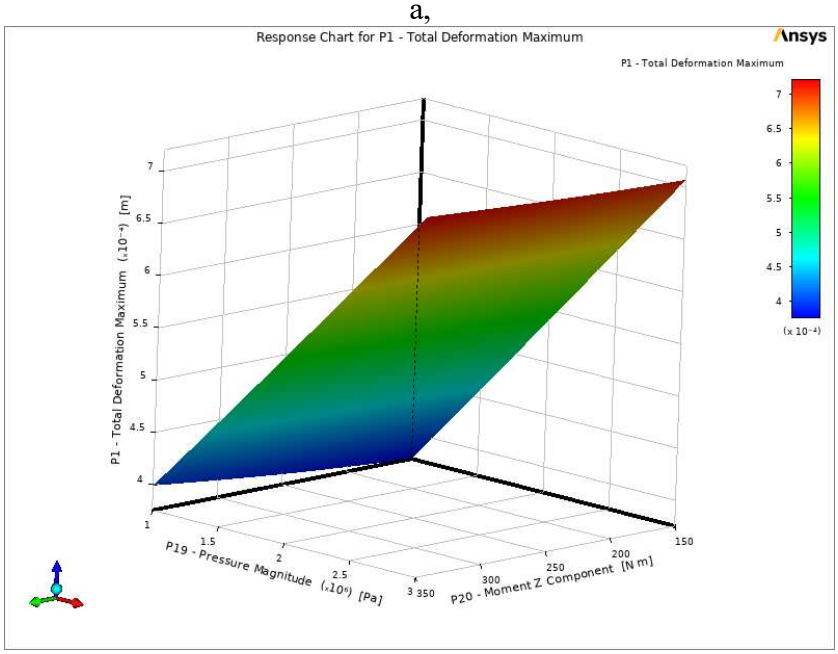
Figure 8. Response surfaces for heat-flux indicators as functions of clamping pressure and friction coefficient: (a) maximum total heat flux; (b) maximum directional heat flux.

Fig. 8 presents the predicted relationships between clamping pressure, friction coefficient, and the selected heat-flux responses. The surfaces can be used to examine how the predicted heat-

flux indicators change when pressure and friction coefficient vary together. The numerical values should be interpreted according to the definitions and units of the corresponding ANSYS output parameters. The physical interpretation of these surfaces depends on how frictional heating was implemented in the finite-element model. For a model in which interfacial frictional heat generation is explicitly calculated, the local heat-generation rate per unit area is commonly related to friction coefficient, contact pressure, and relative sliding speed. However, this relationship should not be treated as a direct description of the current simulation unless the implemented thermal-loading procedure uses those quantities to calculate the heat input.



a,



b,

Figure 9. Response surfaces for (a) maximum temperature and (b) maximum assembly deformation as functions of clamping pressure and applied torque.

Fig. 9 illustrates the metamodelled variation in maximum temperature and maximum assembly deformation with clamping pressure and applied torque. The surfaces provide a visual means of identifying regions associated with higher or lower predicted responses and can help guide the selection of candidate operating conditions. The temperature data in Table 3 show that some sampled conditions produced temperatures above 400°C, with the highest sampled value reaching 456.83°C at DP9. These values identify thermally demanding conditions within the investigated design space. They do not, without additional material-specific evidence, establish that the composite has failed or that permanent degradation has occurred.

Similarly, the response surfaces should not be interpreted as proof of a unique global optimum. They represent metamodel predictions constructed from the specified design variables and simulation results. Their main purpose in this study is to support design-space exploration and the subsequent constrained optimization.

5.6. Multi-Objective Constraint-Based Optimization and FEA Verification

A multi-objective optimization procedure was considered to identify operating conditions that reduce both maximum assembly deformation and maximum temperature. The decision vector was defined as:

$$\mathrm{x} = [P_{19}, P_{20}, P_{21}] \tag{11}$$

where P_{19} is clamping pressure, P_{20} is applied torque, and P_{21} is the friction coefficient. The optimization problem can be expressed as:

$$\min_{\mathrm{x}}\{Y_1(\mathrm{x}), Y_2(\mathrm{x})\} \quad \text{subject to:} \quad \begin{cases} 1 \le P_{19} \le 3\ \mathrm{MPa} \\ 150 \le P_{20} \le 350\ \mathrm{N \cdot m} \\ 0.25 \le P_{21} \le 0.40 \\ Y_2(\mathrm{x}) \le 250°\mathrm{C} \end{cases} \tag{12}$$

where Y_1 is maximum assembly deformation and Y_2 is maximum temperature. The temperature condition is treated as a study-imposed constraint. No additional numerical deformation limit is specified here because a verified limit was not provided. The reported MOGA candidate used a clamping pressure of 1.50 MPa, an applied torque of 320 N·m, and a friction coefficient of 0.325. These values correspond to the baseline reference condition, DP0. Direct FEA at this condition produced a maximum temperature of 204.31°C and a maximum total deformation of 0.47016 mm. Relative to the imposed temperature threshold of 250°C, the baseline condition had a temperature margin of

$$\Delta\mathrm{T} = 250 - 204.31 = 45.69°\mathrm{C} \tag{13}$$

Thus, the baseline result satisfied the specified thermal constraint. This comparison establishes feasibility with respect to the imposed temperature threshold, but it does not

alone demonstrate that the reported point is the unique or global optimum of the multi-objective problem. Because the reported MOGA candidate coincides with the baseline condition, its optimization status must be interpreted with caution. A multi-objective procedure typically yields a set of non-dominated solutions; thus, identifying a single preferred candidate requires a predefined selection criterion or constraint set. While the available data justifies selecting the baseline condition, asserting global optimality would require analyzing the optimizer's complete Pareto front and validating the corresponding metamodel predictions.

For rigorous verification, the response-surface predictions at the selected candidate should be compared against direct FEA results using the same input values. The relative error for each response can be evaluated as:

$$\varepsilon_i(\%) = \frac{|Y_{i,\mathrm{RRR}} - Y_{i,\mathrm{FFA}}|}{|Y_{i,\mathrm{FFA}}|} \times 100\% \tag{14}$$

However, because both predicted and simulated values are not simultaneously available at this stage, this numerical validation error is omitted. In conclusion, the 30-point LHS-OSF simulation matrix establishes a robust numerical foundation for the response-surface analysis, sensitivity assessment, and constrained optimization. The sampled data exhibits substantial variations in both temperature and deformation across the operating range. Furthermore, while the metamodel statistics indicate close agreement with the simulation data and the thermal constraint provides a clear screening criterion, further cross-validation between the metamodel and direct simulation is essential before quantifying the optimization accuracy or confirming a globally optimal solution.

6. CONCLUSIONS

This study combined representative volume element (RVE)-based homogenization, finite element analysis (FEA), response surface methodology (RSM), and multi-objective optimization to investigate the thermo-mechanical responses of an automotive dry clutch assembly incorporating a PMC-M1-25 composite friction lining. The main conclusions are summarized as follows.

Material homogenization: RVE-based homogenization was used to estimate the effective thermo-mechanical properties of the composite containing 25 vol.% Al_2O_3 particles. The resulting properties were assigned to the macro-scale finite element model for subsequent thermo-mechanical analysis.

Thermo-mechanical responses: Across the 30 LHS-OSF design points, the maximum predicted temperature was 456.83 °C at DP9, whereas the maximum assembly

deformation was 0.698 mm at DP25. The sampled results demonstrate considerable variation in the predicted responses across the investigated ranges of clamping pressure, applied torque, and friction coefficient.

Metamodel performance and parameter sensitivity: The developed response-surface models achieved R^2 values ranging from 0.9946 to 0.9986 for the reported responses. The sensitivity analysis identified clamping pressure as an important parameter affecting the predicted deformation and thermal responses, while the friction coefficient also contributed to the thermal response. These findings apply to the investigated parameter ranges and the numerical model used in this study.

Evaluation of the selected operating condition: At a clamping pressure of 1.50 MPa, an applied torque of 320 N·m, and a friction coefficient of 0.325, direct FEA yielded a maximum temperature of 204.31 °C and a maximum assembly deformation of approximately 0.470 mm. The predicted temperature was 45.69 °C below the imposed thermal constraint of 250 °C. This result confirms compliance with the specified temperature criterion at the selected condition, but does not independently establish a globally optimal solution.

Overall, the proposed numerical framework provides a systematic approach for examining thermo-mechanical responses and screening operating conditions for an automotive dry clutch assembly with a composite friction lining. Future work should incorporate temperature-dependent material properties, repeated clutch engagement cycles, and experimental validation to assess the predictive accuracy of the numerical model under practical operating conditions.

Declarations

Open Access

I confirm that I understand Scientific Reports is an open access journal that levies an article processing charge per articles accepted for publication. By submitting my article I agree to pay this charge in full if my article is accepted for publication.

Competing Interests

No, I declare that the authors have no competing interests as defined by Nature Research, or other interests that might be perceived to influence the results and/or discussion reported in this paper.

Dual Publication

The results/data/figures in this manuscript have not been published elsewhere, nor are they under consideration (from you or one of your Contributing Authors) by another publisher.

Authorship

I have read the Nature Portfolio journal policies on author responsibilities and submit this

manuscript in accordance with those policies.

Third Party Material

All of the material is owned by the authors and/or no permissions are required.

Data Availability

Yes, I have research data to declare.

All data generated or analysed during this study are included in this published article.

Funding

The authors received no financial support for the research, authorship, and/or publication of this article.

REFERENCES

[1] Jabbar, N. A., Hussain, I. Y., & Abdullah, O. I. (2021). Thermal and thermoelastic problems in dry friction clutch: A comprehensive review. *Heat Transfer, 50*(8), 7855–7878. https://doi.org/10.1002/htj.22257

[2] Pisaturo, M., & Senatore, A. (2016). Simulation of engagement control in automotive dry-clutch and temperature field analysis through finite element model. *Applied Thermal Engineering, 93*, 958–966. https://doi.org/10.1016/j.applthermaleng.2015.10.068

[3] Abdullah, O. I., Abd Al-Sahb, W., & Al-Shabibi, A. (2015). Finite element analysis of transient thermoelastic behavior in multi-disc clutches. *SAE Technical Paper 2015-01-0676*. https://doi.org/10.4271/2015-01-0676

[4] Bezzazi, M., Khamlichi, A., Jabbouri, A., Reis, P., & Davim, J. P. (2007). Experimental characterization of frictional behaviour of clutch facings using Pin-on-disk machine. *Materials & Design, 28*(7), 2148–2153. https://doi.org/10.1016/j.matdes.2006.07.001

[5] Ouyang, Y., Bai, L., Tian, H., Li, X., & Yuan, F. (2022). Recent progress of thermal conductive polymer composites: Al_2O_3 fillers, properties and applications. *Composites Part A: Applied Science and Manufacturing, 152*, 106685. https://doi.org/10.1016/j.compositesa.2021.106685

[6] Adem, A. A., Panjiar, H., & Daniel, B. S. S. (2024). The effect of nanocarbon inclusion on mechanical, tribological, and thermal properties of phenolic resin-based composites: An overview. *Engineering Reports, 6*(4), e12861. https://doi.org/10.1002/eng2.12861

[7] Chan, D., & Stachowiak, G. W. (2004). Review of automotive brake friction materials. *Proceedings of the Institution of Mechanical Engineers, Part D: Journal of Automobile Engineering, 218*(9), 953–966. https://doi.org/10.1243/0954407041856773

[8] Blau, P. J. (2008). *Friction Science and Technology: From Concepts to Applications* (2nd ed.). CRC Press.

[9] Xiong, X., Shen, S. Z., Hua, L., Liu, J. Z., Li, X., Wan, X., & Miao, M. (2018). Finite element models of natural fibers and their composites: A review. *Journal of Reinforced Plastics and Composites, 37*(9), 617–635. https://doi.org/10.1177/0731684418755552

[10] Hill, R. (1963). Elastic properties of reinforced solids: Some theoretical principles. *Journal of the Mechanics and Physics of Solids, 11*(5), 357–372. https://doi.org/10.1016/0022-5096(63)90036-X

[11] Hashin, Z. (1983). Analysis of composite materials—A survey. *Journal of Applied Mechanics, 50*(3), 481–505. https://doi.org/10.1115/1.3167081

[12] Terada, K., & Kikuchi, N. (2001). A class of general algorithms for multi-scale analyses of heterogeneous media. *Computer Methods in Applied Mechanics and Engineering, 190*(40–41), 5427–5464. https://doi.org/10.1016/S0045-7825(01)00179-7

[13] Ansys, Inc. Ansys Material Designer User's Guide, Release 2025 R2. Canonsburg, PA: Ansys, Inc., 2025.

[14] McKay, M. D., Beckman, R. J., & Conover, W. J. (1979). A comparison of three methods for selecting values of input variables in the analysis of output from a computer code. *Technometrics, 21*(2), 239–245. https://doi.org/10.1080/00401706.1979.10489755

[15] Morris, M. D., & Mitchell, T. J. (1995). Exploratory designs for computational experiments. *Journal of Statistical Planning and Inference, 43*(3), 381–402. https://doi.org/10.1016/0378-3758(94)00035-T

[16] Box, G. E. P., & Wilson, K. B. (1951). On the experimental attainment of optimum conditions. *Journal of the Royal Statistical Society: Series B (Methodological), 13*(1), 1–38. https://doi.org/10.1111/j.2517-6161.1951.tb00067.x

[17] Myers, R. H., Montgomery, D. C., & Anderson-Cook, C. M. (2016). *Response Surface Methodology: Process and Product Optimization Using Designed Experiments* (4th ed.). Wiley.

[18] Montgomery, D. C. (2017). *Design and Analysis of Experiments* (9th ed.). Wiley.

[19] Box, G. E. P., & Draper, N. R. (1987). *Empirical Model-Building and Response Surfaces*. Wiley.

[20] Jones, D. R., Schonlau, M., & Welch, W. J. (1998). Efficient global optimization of expensive black-box functions. *Journal of Global Optimization, 13*, 455–492. https://doi.org/10.1023/A:1008306431147

[21] Ansys, Inc. Ansys DesignXplorer User Documentation, Release 2025 R2. Canonsburg, PA: Ansys, Inc., 2025.

[22] Sobol, I. M. (2001). Global sensitivity indices for nonlinear mathematical models and their Monte Carlo estimates. *Mathematics and Computers in Simulation, 55*(1–3), 271–280. https://doi.org/10.1016/S0378-4754(00)00270-6

[23] Saltelli, A., Ratto, M., Andres, T., Campolongo, F., Cariboni, J., Gatelli, D., Saisana, M., & Tarantola, S. (2008). *Global Sensitivity Analysis: The Primer*. Wiley.

[24] Deb, K., Pratap, A., Agarwal, S., & Meyarivan, T. (2002). A fast and elitist multiobjective genetic algorithm: NSGA-II. *IEEE Transactions on Evolutionary Computation, 6*(2), 182–197. https://doi.org/10.1109/4235.996017

[25] Coello Coello, C. A. (2006). Evolutionary multi-objective optimization: A historical view of the field. *IEEE Computational Intelligence Magazine, 1*(1), 28–36. https://doi.org/10.1109/MCI.2006.1597059

[26] Trinh, P.H.; Thanh, D.V. Parametric Multiscale Homogenization and Coupled Thermo-Structural Analysis of Hybrid Al–SiC–Gr Brake Discs via Sequential Micromechanical Modeling. *J. Compos. Sci.* **2026**, *10*, 453. https://doi.org/10.3390/jcs10090453

[27] Jabbar, N. A., Hussain, I. Y., & Abdullah, O. I. (2021). Thermal and thermoelastic problems in dry friction clutch: A comprehensive review. *Heat Transfer, 50*(8), 7855–7878. https://doi.org/10.1002/htj.22257

[28] Pisaturo, M., & Senatore, A. (2016). Simulation of engagement control in automotive dry-clutch and temperature field analysis through finite element model. *Applied Thermal Engineering, 93*, 958–966. https://doi.org/10.1016/j.applthermaleng.2015.10.068